

ON THE GROWTH RATE OF PLASMOID CHAINS DURING NONLINEAR VISCORESISTIVE EVOLUTION OF THE TILT INSTABILITY

HUBERT BATY

Observatoire Astronomique de Strasbourg, Université de Strasbourg, CNRS, UMR 7550, 11 rue de l'Université, F-67000 Strasbourg, France

ABSTRACT

We investigate by means of two-dimensional incompressible magnetohydrodynamic (MHD) numerical simulations, the onset phase of the fast collisional magnetic reconnection regime that is supported by the formation of plasmoid chains when the Lundquist number S exceeds a critical value. The present study extends previous results obtained at magnetic Prandtl number $P_m = 1$ (Baty 2020) to a range of different P_m values. We use FINMHD code where a set of reduced visco-resistive MHD equations is employed to form two quasi-singular current layers as a consequence of the tilt instability. The results reinforce the conclusion that, a phase of sudden super-Alfvénic growth (when P_m is not too high) of plasmoid chains is obtained, following a previous quiescent phase during current sheet formation on a slower Alfvénic time scale. We compare our results with predictions from the general theory of the plasmoid instability. We also discuss the importance of this onset phase to reach the ensuing stochastic time-dependent reconnection regime, where a fast time-averaged rate independent of S is obtained. Finally, we briefly discuss the relevance of our results to explain the flaring activity in solar corona and internal disruptions in tokamaks.

Keywords: magnetic reconnection — magnetohydrodynamics — plasmas — stars: coronae — Sun: flares

1. MOTIVATION

Magnetic reconnection is believed to be the underlying mechanism that explains explosive events observed in many magnetically dominated plasmas. This is for example the case for flares in the solar corona, or sawtooth crashes in tokamaks. It is a process of topological rearrangement of magnetic field lines that can convert a part of the magnetic energy into kinetic energy and heat (Priest & Forbes 2000). However, the timescales involved in classical two-dimensional (2D) reconnection models within the macroscopic magnetohydrodynamic (MHD) regime are too slow to match the observations or experiments. Indeed, the reconnection rate predicted by Sweet-Parker (SP) model which scales like $S^{-1/2}$ (S being the Lundquist number defined as $S = LV_A/\eta$, where L is the half-length of the current sheet, V_A is the Alfvén speed based on the magnetic field amplitude in the upstream current layer, and η is the resistivity), is too low by a few (or even many) orders of magnitude for the relevant Lundquist numbers (Sweet 1958; Parker 1957). For example, for typical parameters representative of the solar corona, S is of order 10^{12} , leading to a normalized reconnection rate of order 10^{-6} much lower than the value of $10^{-2} - 10^{-1}$ required to match the observations. Furthermore, SP theory assumes a steady-state process that cannot explain the impulsive (thus even faster) onset phase preceding the main one.

However, it has been realized in the last decade that, even in a magnetofluid approach, a new solution with a rate that is (possibly) fast enough and almost independent on S can be obtained, provided that S is higher than a critical value of order 10^4 . This new regime is supported by the formation of plasmoid chains disrupting the current sheet in which they are born, as obtained in many numerical experiments (Samtaney et al. 2009; Bhattacharjee et al. 2009; Huang & Bhattacharjee 2010). More precisely, these plasmoids are small magnetic islands due to tearing-type resistive instabilities, constantly forming, moving, eventually coalescing, and finally being ejected through the outflow boundaries. At a given time, the system appears as an aligned layer structure of plasmoids of different sizes, and can be regarded as a statistical steady state with a time-averaged reconnection rate that is nearly (or exactly)

independent of the dissipation parameters (Uzdensky et al. 2010; Loureiro et al. 2012). The modal linear theory of plasmoid instability is based on a preformed static (i.e. reconnection flows effects are neglected) unstable SP current sheet with a half-width $a \simeq LS^{-1/2}$ (Loureiro et al. 2007). Among the spectrum of many unstable modes (as $ka \leq 1$ is required if we assume a Harris-type current layer profile having a hyperbolic tangent magnetic field reversal), the linearly dominant wavenumber k_p follows $k_p L \simeq 1.4 (1 + P_m)^{-3/16} S^{3/8}$ (where $P_m = \nu/\eta$ is the magnetic Prandtl number, i.e. the ratio of the viscosity coefficient ν to the resistivity one η) with a corresponding maximum linear growth rate γ_p scaling as $\gamma_p \tau_A \simeq 0.62 (1 + P_m)^{-5/8} S^{1/4}$, where $\tau_A = L/V_A$ is the Alfvén time based on the current sheet half-length (Comisso & Grasso 2016; Huang et al. 2019).

Beyond these above well admitted results and despite many published papers on the subject, there is no clear consensus on a theoretical view for the plasmoids-reconnection regime including the onset phase.

The paradoxical result of infinite linear growth rate (see scaling law just above) in an ideal MHD plasma (i.e. infinite S) being incompatible with the frozen-in condition that makes reconnection impossible, an issue has been proposed by considering unstable current layers having a critical aspect ratio $L/a \simeq S^\alpha$, that is smaller than SP value in the high S limit as $0.25 < \alpha < 0.5$ (Pucci & Velli 2014). In this way, the linear growth rate becomes Alfvénic and independent of S . The value of the exponent α depends on the current profile (Pucci et al. 2018). For example, $\alpha = 1/3$ is found for the standard Harris current profile, leading to $\gamma_p \tau_A \simeq 0.62$ (case of zero viscosity) with the corresponding linearly dominant wavenumber k_p following the relation $k_p L \simeq 1.4 S^{1/6}$. These results have been confirmed by numerical simulations of preformed static current layers having the correct aspect ratio value, and seem to remain true when extended to macroscopic current sheets of fixed length that are artificially forced to collapse asymptotically towards $a/L \sim S^{-1/3}$ and $a/L \sim S^{-1/2}$ on a time scale of order of τ_A (Tenerani et al. 2015, 2016).

On the other hand, a second theoretical issue has been proposed by Comisso et al. (2016, 2017) by investigating the plasmoid instability in a dynamically evolving (exponentially shrinking in time and reaching asymptotically a SP aspect ratio) current sheet. Without any assumption on the critical current sheet aspect ratio for disruption onset, they employ a principle of least time to derive it as well as the corresponding dominant mode and associated growth rate. The main difference compared to the approach proposed by the first issue, is that the dominant mode is not necessarily the linearly fastest one (obtained from a classical static stability study), but the mode that is able to emerge first at the end of the linear phase. In this way, new scalings that are not simple S -power laws are obtained. For example, the dominant mode growth rate is predicted to follow a transition between the previous scaling $\gamma_p \propto S^{1/4}$ (for moderate S values, $S \gtrsim S_c$) and an asymptotic (for very high S values, $S \gg S_c$) new scaling with a decreasing logarithmic dependence (see Equation 19 in Comisso et al. (2016), and Equation 32 in Comisso et al. (2017)). The growth rate can in principle easily attain super-Alfvénic values $\gamma_p \tau_A \sim 10 - 100$, while remaining finite in the infinite S limit. The precise value of the growth rate and of the corresponding wavenumber also depend on other parameters than S , that are the characteristic time scale of the current sheet formation, the thinning process, the magnetic Prandtl number, and the noise of the system.

This second issue seems to be partly supported by recent 2D numerical MHD simulations, where the coalescence instability between two parallel currents is chosen as the initial setup providing the thinning process to form the current sheet (Huang et al. 2017). Indeed, a scaling law transition is effectively observed, and maximum growth rates with $\gamma_p \tau_A \simeq 10 - 20$ are obtained that are substantially smaller than values predicted by the theoretical model. The remaining differences between the simulations and the analytical model of Comisso et al. (2016, 2017) are explained by taking into account the effects of the reconnection outflow in a phenomenological model (Huang et al. 2019). In our previous study using a different setup (Baty 2020) (hereafter denoted as Paper I), namely using the tilt instability between two repelling antiparallel currents (Richard et al. 1990), a similar conclusion was drawn with obtained maximum super-Alfvénic growth rates $\gamma_p \tau_A \simeq 10$.

Conversely, as the first theoretical model proposed by Pucci & Velli (2014) predicts constant and smaller growth rates, more precisely with $\gamma_p \tau_A \sim 1$, it consequently seems to fail to explain these numerical simulations based on coalescence/tilt setups. However, when submitting the results of Paper I, a controversial point arises about validity of the diagnostic (i.e. the maximum current density) used to estimate the growth rate at which plasmoids can grow. In the present work, we thus focus on this onset phase leading to the disruption of the current sheets by the formation of many plasmoids. Using the same MHD code (FINMHD, Baty (2019)) and numerical procedure with the tilt instability setup, we extend the results obtained in Paper I at $P_m = 1$, for a range of different P_m values. The ensuing statistical steady state with a fast reconnection rate is beyond the scope of the present paper and is left to a future work. The outline of the paper is as follows. In section 2, we present the MHD code and the initial setup for tilt instability. Section 3 is devoted to the presentation of the results. Finally, we conclude in section 4.

2. THE MHD CODE AND INITIAL SETUP

2.1. FINMHD equations

For FINMD, a set of reduced MHD equations has been chosen corresponding to a 2D incompressible model. However, instead of taking the usual formulation with vorticity and magnetic flux functions for the main variables, another choice using current-vorticity ($J - \omega$) variables is preferred because of its more symmetric formulation, facilitating the numerical matrix calculus. The latter choice also cures numerical difficulty due to the numerical treatment of a third order spatial derivative term (Philip et al. 2007). To summarize, the following set of equations is (see also Baty (2019) for more details),

$$\frac{\partial \omega}{\partial t} + (\mathbf{V} \cdot \nabla) \omega = (\mathbf{B} \cdot \nabla) J + \nu \nabla^2 \omega, \quad (1)$$

$$\frac{\partial J}{\partial t} + (\mathbf{V} \cdot \nabla) J = (\mathbf{B} \cdot \nabla) \omega + \eta \nabla^2 J + g(\phi, \psi), \quad (2)$$

$$\nabla^2 \phi = -\omega, \quad (3)$$

$$\nabla^2 \psi = -J, \quad (4)$$

with $g(\phi, \psi) = 2 \left[\frac{\partial^2 \phi}{\partial x \partial y} \left(\frac{\partial^2 \psi}{\partial x^2} - \frac{\partial^2 \psi}{\partial y^2} \right) - \frac{\partial^2 \psi}{\partial x \partial y} \left(\frac{\partial^2 \phi}{\partial x^2} - \frac{\partial^2 \phi}{\partial y^2} \right) \right]$. As usual, we have introduced the two stream functions, $\phi(x, y)$ and $\psi(x, y)$, from the fluid velocity $\mathbf{V} = \nabla \phi \wedge \mathbf{e}_z$ and magnetic field $\mathbf{B} = \nabla \psi \wedge \mathbf{e}_z$ (\mathbf{e}_z being the unit vector perpendicular to the xOy simulation plane). J and vorticity ω are the z components of the current density and vorticity vectors, as $\mathbf{J} = \nabla \wedge \mathbf{B}$ and $\boldsymbol{\omega} = \nabla \wedge \mathbf{V}$ respectively (with units using $\mu_0 = 1$). Note that we consider the resistive diffusion via the $\eta \nabla^2 J$ term (η being assumed uniform for simplicity), and also a viscous term $\nu \nabla^2 \omega$ in a similar way (with ν being the viscosity parameter also assumed uniform). The above definitions results from the choice $\psi \equiv A_z$, where A_z is the z component of the potentiel vector \mathbf{A} (as $\mathbf{B} = \nabla \wedge \mathbf{A}$). This choice is the one used in Ng et al. (2007) or in Baty & Nishikawa (2016), and different from the one used by Lankalapalli et al. (2007) where the choice $\psi \equiv -A_z$ is done. In the latter case, the two Poisson equations (i.e. Equations 3-4) involve an opposite sign in the right hand sides. Note that thermal pressure gradient is naturally absent from our set of equations. Note also that, an advantage of the above formulation over a standard one using the velocity and magnetic field vectors (\mathbf{V}, \mathbf{B}) as the main variables, is the divergence-free property naturally ensured for these two vectors.

2.2. FINMHD numerical method

Simulating the mechanism of magnetic reconnection in the high Lundquist number regime requires the use of particularly well adapted methods. Conventional codes generally lack some convergence properties to follow the associated complicated time dependent bursty dynamics (Keppens et al. 2013). Despite the fact that they are not commonly used, finite element techniques allows to treat the early formation of quasi-singularities (Strauss & Longcope 1998; Lankalapalli et al. 2007), and the ensuing magnetic reconnection in an efficient way (Baty 2019).

FINMHD code is based on a finite element method using triangles with quadratic basis functions on an unstructured grid. A characteristic-Galerkin scheme is chosen in order to discretize in a stable way the Lagrangian derivative $\frac{\partial}{\partial t} + (\mathbf{V} \cdot \nabla)$ appearing in the two first equations (Baty 2019). Moreover, a highly adaptive (in space and time) scheme is developed in order to follow the rapid evolution of the solution, using either a first-order time integrator (linearly unconditionally stable) or a second-order one (subject to a CFL time-step restriction). Typically, a new adapted grid can be computed at each time step, by searching the grid that renders an estimated error nearly uniform. The finite elements Freefem++ software allows to do this (Hecht 2012), by using the Hessian matrix of a given function (taken to be the current density in this study). The technique used in FINMHD has been tested on challenging tests, involving unsteady strongly anisotropic solution for the advection equation, formation of shock structures for viscous Burgers equation, and magnetic reconnection for the reduced set of MHD equations. The reader should refer to Baty (2019) for more details.

2.3. The initial setup

The initial magnetic field configuration for tilt instability is a dipole current structure similar to the dipole vortex flow pattern in fluid dynamics (Richard et al. 1990). It consists of two oppositely directed currents embedded in a constant magnetic field. Contrary to the coalescence instability based on attracting parallel current structures, the two

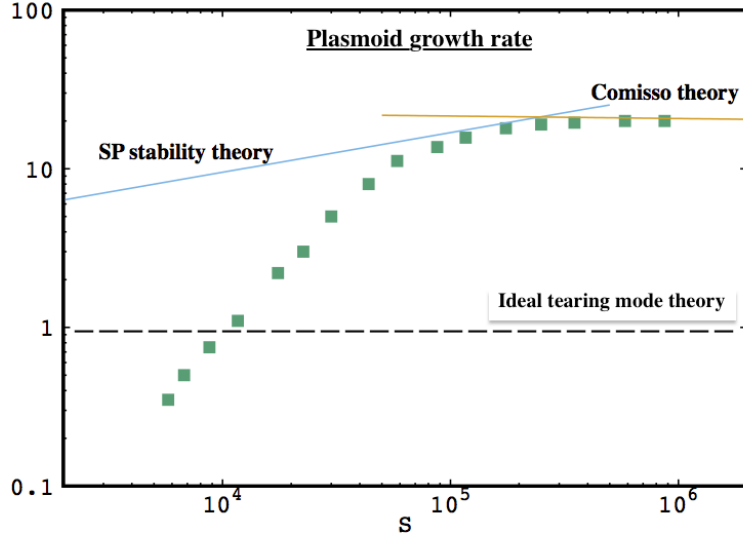


Figure 1. Growth rate $\gamma_p t_A$ obtained for plasmoid formation in simulations at different S for $P_m = 1$ (squares), expected from SP linear theory scaling as $0.9 \times S^{1/4}$, expected from asymptotic solutions of Comisso et al. having a decreasing logarithmic dependence, and deduced from theoretical model of the ideal tearing mode proposed by Pucci & Velli. Note that, only the regime where plasmoids can form is considered, as $S \gtrsim S_c$ (with $S_c \simeq 5 \times 10^3$). Growth rate values using τ_A for normalization can be deduced as $\gamma_p \tau_A \simeq \gamma_p t_A / 2$.

antiparallel currents in the configuration tend to repel. The initial equilibrium is thus defined by taking the following magnetic flux distribution,

$$\psi_e(x, y) = \begin{cases} \left(\frac{1}{r} - r \right) \frac{y}{r} & \text{if } r > 1, \\ -\frac{2}{\alpha J_0(\alpha)} J_1(\alpha r) \frac{y}{r} & \text{if } r \leq 1. \end{cases} \quad (5)$$

And the corresponding current density is,

$$J_e(x, y) = \begin{cases} 0 & \text{if } r > 1, \\ -\frac{2\alpha}{J_0(\alpha)} J_1(\alpha r) \frac{y}{r} & \text{if } r \leq 1, \end{cases} \quad (6)$$

where $r = \sqrt{x^2 + y^2}$, and J_0 et J_1 are Bessel functions of order 0 and 1 respectively. Note also that α is the first (non zero) root of J_1 , i.e. $\alpha = 3.83170597$. This initial setup is similar to the one used in the previously cited references (Richard et al. 1990), and rotated with an angle of $\pi/2$ compared to the equilibrium chosen in the other studies (Keppens et al. 2014). Note that, the asymptotic (at large r) magnetic field strength is unity, and thus defines our normalisation. Consequently, our unit time in the following paper, will be defined as the Alfvén transit time across the unit distance (i.e. the initial characteristic length scale of the dipole structure) as $t_A = 1$. The latter time is slightly different from τ_A that is based on the half-length of the current sheet and on the upstream magnetic field magnitude. However, in our simulations we can deduce that $\tau_A \simeq t_A/2$ (see below and Paper I). In usual MHD framework using the flow velocity and magnetic variables, force-free equilibria using an additional vertical (perpendicular to the $x - y$ plane) can be considered (Richard et al. 1990), or non force-free equilibria can be also ensured trough a a thermal pressure gradient balancing the Lorentz force (Keppens et al. 2014). In our incompressible reduced MHD model, as thermal pressure is naturally absent, we are not concerned by such choice.

In previous studies using a similar physical setup, a square domain $[-R : R]^2$ was taken with R large enough in order to have a weak effect on the central dynamics. For example a standard value of $R = 3$ is taken in Baty (2019). In the present work and in Paper I (Baty 2020), a choice of using a circular domain with a radius $R = 3$ is done. We have checked that it does not influence the results compared to the square domain setup. However, this allows the use of a lower number of finite-element triangles (as the circle area is evidently smaller than the square for the same radius value R), and this also simplifies the numerical boundary treatment as only one boundary instead of four in our finite-element discretization are needed.

A stability analysis in the reduced MHD approximation using the energy principle has given that the linear eigen-

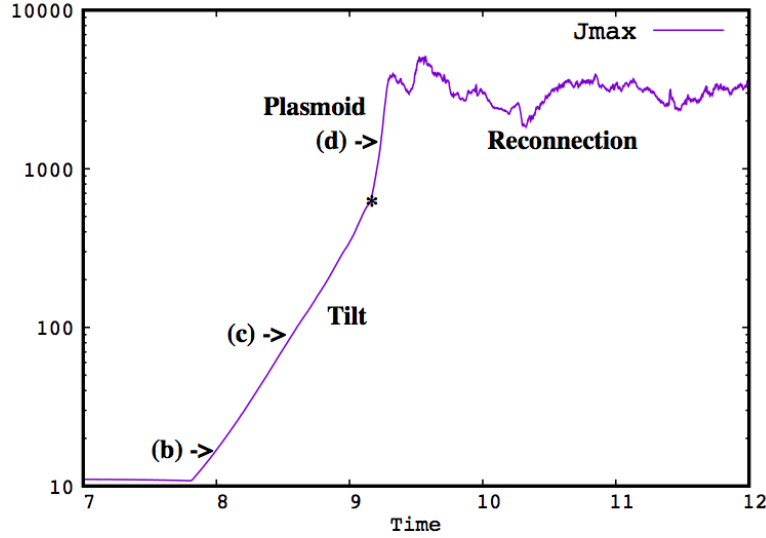


Figure 2. Time history of the maximum current density obtained for a run using $P_m = 1$ and $S^* = 1/\eta = 5 \times 10^4$ (the corresponding Lundquist number is $S \simeq 1 \times 10^5$). The three different phases, namely the tilt development, the plasmoid chains formation, and the stochastic reconnection regime are indicated. The time is normalized using t_A (see text).

function of the tilt mode is a combination of rotation and outward displacement (Richard et al. 1990). Instead of imposing such function in order to perturb the initial setup, we have chosen to let the instability develops from the initial numerical noise. Consequently, an initial zero stream function is assumed $\phi_e(x, y) = 0$, with zero initial vorticity $\omega_e(x, y) = 0$. The values of our four different variables are also imposed to be constant in time and equal to their initial values at the boundary $r = R$.

3. RESULTS

3.1. Summary of the previous study at $P_m = 1$ (Paper I)

First, from our knowledge, this study was the first one to address in detail the reconnection process associated with the nonlinear evolution of the tilt instability. Interesting results, even in the SP (Sweet-Parker) regime were obtained. Indeed, two forming twin current sheets (with current density of opposite sign) drive a steady-state reconnection in agreement with classical scaling laws given by the famous Sweet-Parker model. A slight amendment by a factor of two for the vorticity of the outflow is however required due to the particular asymmetry associated with the curved geometry of the current layers (see Figure 8 in Paper I).

In this latter study using the tilt instability as a triggering mechanism to form the current sheets at magnetic Prandtl number $P_m = 1$, the transition from a SP reconnection process to a plasmoid-dominated regime occurs for a critical Lundquist number $S_c \simeq 5 \times 10^3$. This is a factor of two lower than the often-quoted $S_c \sim 10^4$ value in the literature. However, there is no precise universal value, as it depends on different parameters like, the current sheet geometry (via the choice for the initial setup), the magnetic Prandtl number, and also the noise amplitude (via the numerical scheme). The exact definition of the Lundquist number can also differ slightly from one study to another. For coalescence instability, a value of $S_c \sim 3 \times 10^4$ has been reported in simulations assuming zero explicit viscosity. Even for Lundquist number very slightly lower than S_c , the formation of a transient single plasmoid was observed to occur at a relatively late time, with no real impact on the SP reconnection rate (see Figures 9-10 in Paper I).

In the plasmoid-dominated regime, the growth of the plasmoids has been examined, from their birth to their ensuing disrupting effect on the current sheets. An important reference time scale for comparing the latter growth is the time scale for forming the current layers, that is given by $\tau = 0.38 t_A \sim 1 \tau_A$, as the tilt mode is an ideal MHD instability leading to a current density increasing exponentially as $e^{2.6t}$ (t being expressed in units of t_A). This triggering phase in the simulations has been carefully checked to agree with stability theory (Richard et al. 1990). As seen in Figure 6 of Paper I, the formation of the current sheets proceeds through a combination of thinning (as a is observed to decrease in time), stretching (as L is increasing), and a weak magnetic field strengthening, in agreement with the scenario suggested by Tolman et al. (2018).

In paper I, we have defined two simple parameters characterizing the growth of the forming plasmoids. The first one, t_p , is the delay time between the birth of the first plasmoids (time at which they become to be barely visible

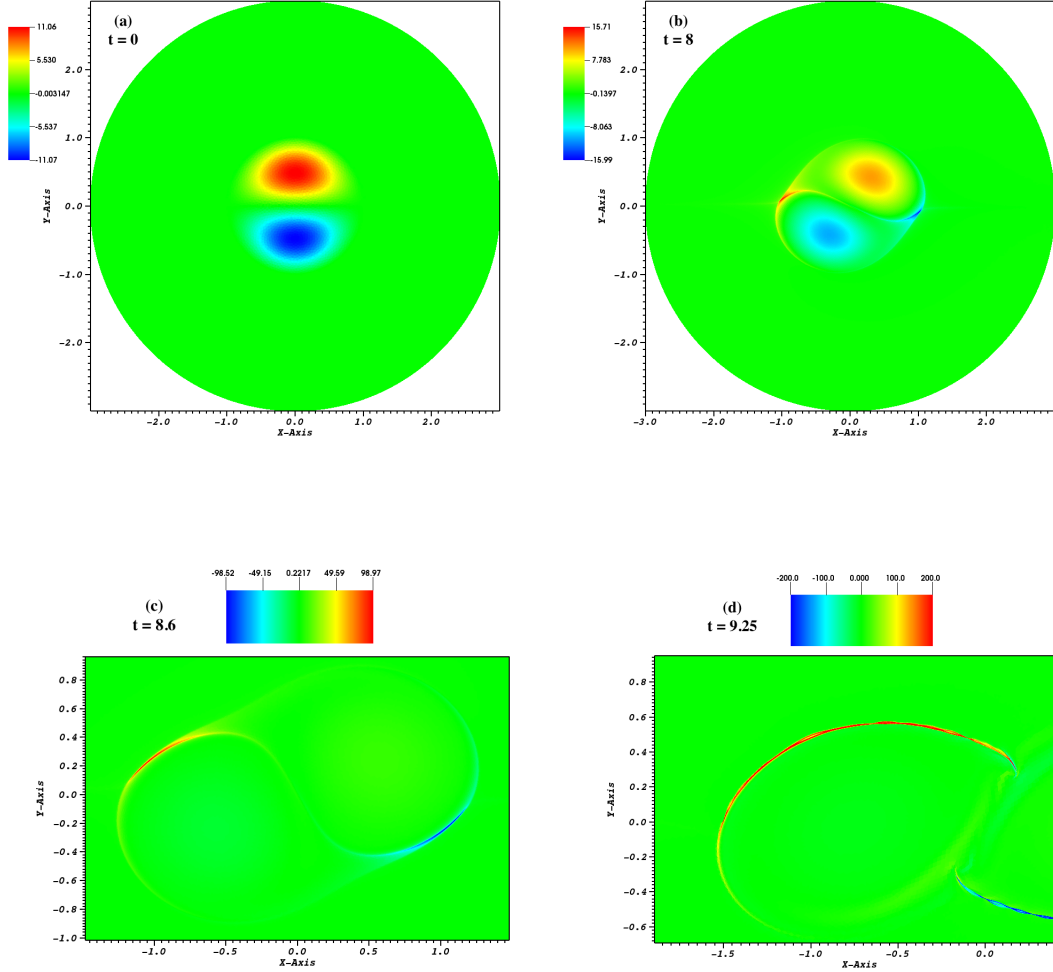


Figure 3. Snapshots of the colored contour map of the current density, corresponding to different times of the previous figure. Note that a zoom-in of the central region is used for (c)-(d), with additionally saturated values in the range $[-200 : 200]$ for (d) case.

in the current density structure) and the start of the formation of the currents sheets (taken as the time at which the corresponding current density exceeds the equilibrium setup value). A rapidly converged constant value (with S) of $t_p = 2.4 \tau_A$ is obtained (see Figure 14 in Paper I). This delay time has been identified to correspond to the quiescent phase proposed in Comisso et al.’s scenario, during which many modes become progressively unstable and compete with each other (see Figures 3-4 in Comisso et al. (2017)). Indeed, the duration of this phase is predicted to be approximatively given by the time scale of the current sheet formation. This is also in agreement with a conclusion drawn in Uzdensky et al. (2016). A similar result has been obtained for the coalescence setup, with a slight difference for the highest S values where their time delay is non-monotonic and increases weakly again (Huang et al. 2017). The second parameter is a growth rate, that is estimated by taking the second slope observed during the increase of the maximum current density (see Figure 11 in Paper I), and thus characterizes an abrupt growth phase following the slower previous quiescent phase. The latter growth rate was identified as γ_p , the growth rate of the dominant mode that emerges ”first” at the end of the linear phase in the theory of Comisso et al. (2017).

As one can see in Figure 1, the results obtained for γ_p in Paper I (using $P_m = 1$) qualitatively agree with a non-monotonic dependence with S , as a consequence of the non-power law dependence with S predicted by theory (Comisso et al. 2017). Moreover, values $\gamma_p \tau_A \simeq 10$ (as $\gamma_p t_A \simeq 20$) are also obtained for the highest S values, thus confirming that $\gamma_p \tau_A \gg 1$ at the end of the linear phase. For $S \gtrsim S_c$, the scaling law given by SP stability theory with $\gamma_p \propto S^{1/4}$ has been only marginally recovered. A very similar result has been obtained for the coalescence setup (Huang et al. 2017). The difference at relatively low S can be largely attributed to the reconnection outflow (neglected in theoretical

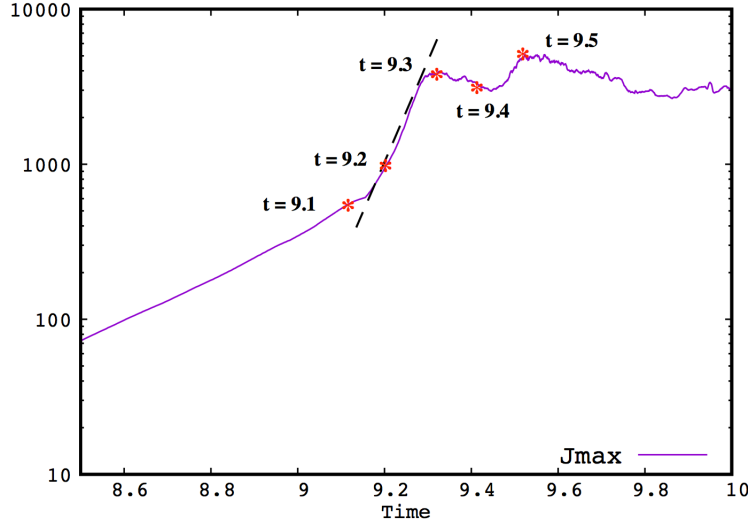


Figure 4. Zoom-in of the time history of the maximum current density obtained for a run using $P_m = 1$ and $S^* = 1/\eta = 5 \times 10^4$, showing the transition between tilt, plasmoid, and reconnection phases.

models) that can affect the growth of the plasmoids and thus the scaling relations (Huang et al. 2019). As shown in previous studies, the noise induced by the numerical simulations also influences the results, and thus is an important parameter that needs to be investigated in future studies. Conversely, our results seem to contradict values deduced from the ideal tearing model of Pucci & Velli (2014), where the linear growth of plasmoids is predicted to be constant and at most Alfvénic (i.e. $\gamma_p t_A \simeq 1$). Indeed, values of $\gamma_p \tau_A \simeq 0.6$ and $\gamma_p \tau_A \simeq 0.4$ are expected at $P_m = 0$ and $P_m = 1$ respectively, assuming an Harris-type profile for the current layer. One must also note that (as explained in introduction), this latter value is obtained by considering the aspect ratio L/a to be equal to the critical value $S^{1/3}$, that is in fact higher during our fast shrinking process of the current sheet (see Figure 16 in Baty (2020)), consequently making possible a higher value.

The use of the time history of the maximum current density in order to estimate the growth rate of the plasmoids in the simulations (as done in our previous study in Paper I) can be criticized. Indeed, we cannot rigorously prove that the relevant phase (called plasmoid phase as one can see below) corresponds to an equivalent phase of linear development of tearing-type instabilities taken from a theoretical stability study of a resistively unstable current layer. In other words, the comparison of our estimated instantaneous growth rate (deduced from the current density time evolution) with the theoretical linear growth rate is not trivial. In the context of the coalescence instability, Huang et al. (2017) separate the fluctuation magnetic field perturbation due to the plasmoid instability from the background field contribution. And, the instantaneous growth rate was consequently derived from the value of the perturbation as a function of time. The use of this technique (via a superposition of Chebyshev polynomials) is possible when the current layer is straight. This is not the case in our study due to the curved nature of the current sheets (see Paper I and figures below in the present paper). Nevertheless, we are able to give two strong arguments reinforcing the use of the maximum current density to estimate γ_p . The first one consists of a close inspection of the current density structure during the plasmoid phase, in order to check when non linear effects associated to the plasmoids growth (like coalescence for example) come into play. The second one consists in doing additional runs at different magnetic Prandtl values, in order to examine the dependence of our estimated γ_p dependence with P_m and compare with dependence predicted from visco-resistive linear theory.

3.2. Detailed time history of the maximum current density obtained at $P_m = 1$

First, in order to have an overview of the time evolution of the system, we have simulated a case using $P_m = 1$ and $S^* = 1/\eta = 5 \times 10^4$. The corresponding Lundquist number $S = LV_A/\eta$ can be deduced by estimating the half length of the current layer L and the magnetic field B_u (as V_A is the Alfvén speed based on the magnetic field amplitude in the upstream current layer B_u), leading to $S \simeq 10^5$.

The results obtained for the measured maximum current density (taken over the whole domain) is plotted in Figure

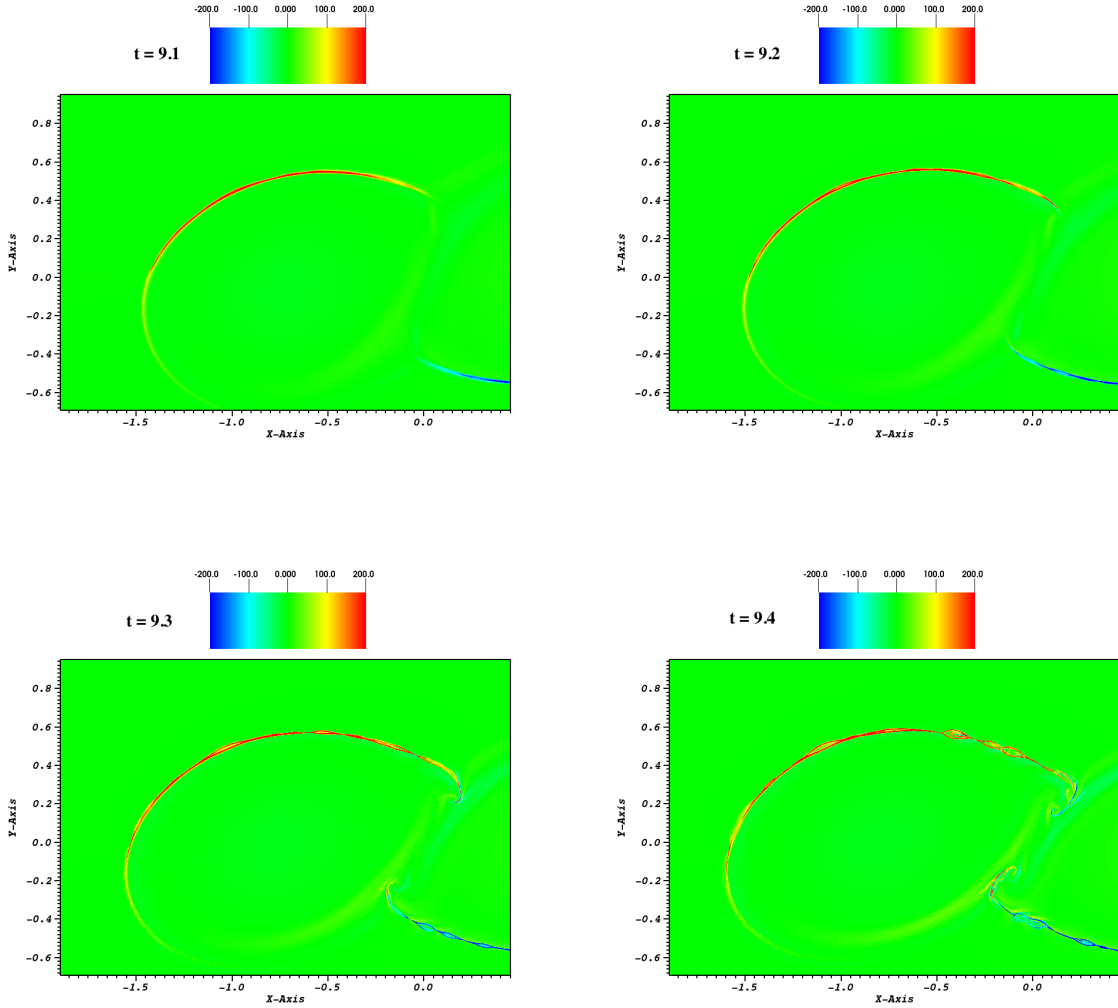


Figure 5. Snapshots of the colored contour map of the current density, corresponding to four different times of the plasmoid growth phase (see previous figure). Note that a zoom-in of the central region (centered on the left current layer) is used with additionally saturated values in the range $[-200 : 200]$.

2 as a function of time. One can see that, at $t \simeq 7.8 t_A$, the tilt instability sets in as two twin current layers are forming (see also Figure 3b). During the tilt phase, the intensity of the density current is increasing in time as $e^{2.6t}$, as described in Paper I (see also Figure 3c for $t = 8.6 t_A$). As the tilt mode is an ideal MHD instability, this phase is not dependent of the resistivity nor of the viscosity (Richard et al. 1990). Later in the time evolution, an abrupt change of slope is clearly visible in Figure 2 at $t \simeq 9.15 t_A$ (at time spotted by the first asterisk). During this slope increase, a chain of plasmoids progressively invades each current layer (see Figure 3d at $t = 9.25 t_A$). The plasmoid phase typically ends when an oscillating quasi stationary phase is obtained with magnetic reconnection taking place (see later).

In paper I, the latter measured current density slope observed during the plasmoid phase was assumed to be a good estimate for the instantaneous growth rate of the plasmoids. In order to check the validity of this assumption, a detailed time history of current layer structure is investigated during the transition between these three phases. The results are plotted in Figures 4-6, for only one of the two current layers for clarity. Indeed, at a time close to the transition between the tilt and plasmoid phases, the plasmoids are barely visible. For example, at $t = 9.1 t_A$, a single plasmoid begins to appear at the right corner of the current layer (see Figure 5a). Then, at $t = 9.2 t_A$ (Figure 5b), other plasmoids begin to appear all along the layer. At $t = 9.3 t_A$, the same plasmoids previously described have grown. Finally at $t = 9.4 t_A$, the plasmoids begin to coalesce (see right corner in Figure 5d) indicating a non

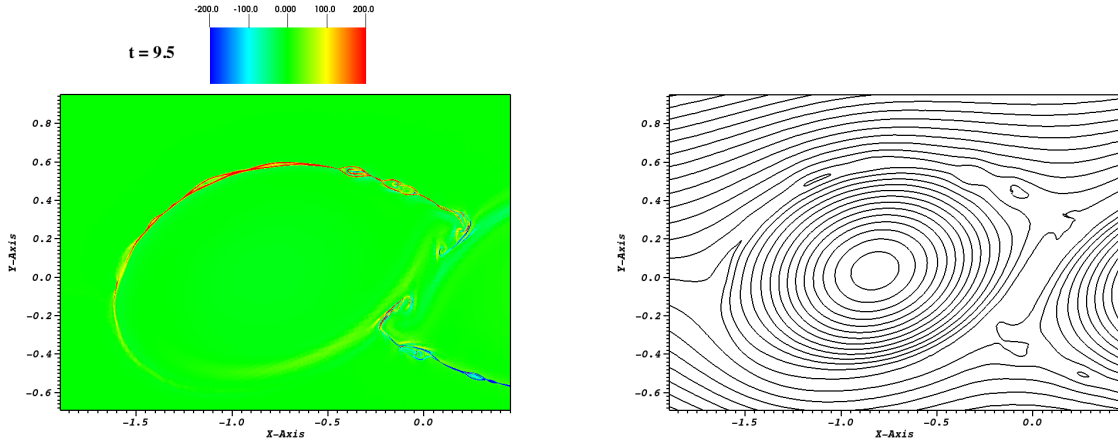


Figure 6. (Left panel) Snapshot of the colored contour map of the current density (centered on the left current layer), corresponding to an early time of the reconnection phase. (Right panel) Corresponding magnetic field lines obtained at the same time.

linear interaction for plasmoid dynamics. The latter coalescence is visible just after (see Figure 6a), and magnetic reconnection is also at work at this time (Figure 6b).

We can conclude that during the plasmoid phase (i.e. between $t = 9.1 t_A$ and $t = 9.3 t_A$) used to determine the growth rate γ_p , the structure of the current layers does not show any non linear behavior. Non linear effects (coalescence between primary islands) begin to be visible only at $t \simeq 9.4 t_A$, thus validating our procedure.

3.3. Simulations at different P_m values

The dependence of the plasmoid growth rate with the Prandtl number P_m is investigated for two inverse resistivity values, taking $S^* = 10^5$ and $S^* = 2 \times 10^4$ in the simulations. Note that, these two values of S^* can be translated into the two corresponding Lundquist number values, $S \simeq 2 \times 10^5$ and $S \simeq 4 \times 10^4$ respectively. The results that are reported in Figure 7, clearly follow a fitted scaling law $\gamma_p \propto (1 + P_m)^{-5/8}$. This is in agreement with predictions from linear theory, as for example $\gamma_p \tau_A \simeq 0.62 (1 + P_m)^{-5/8} S^{1/4}$ derived in [Comisso & Grasso \(2016\)](#). Consequently, it is very unlikely that the second slope increase of the maximum current density is a non linear effect. Otherwise, it would give another P_m dependence with a probably less sensitivity to viscosity.

4. CONCLUSION

In this work, we have extended a previous study (see Paper I) devoted to the formation of chains of plasmoid during magnetic reconnection in the 2D MHD framework. More precisely, the focus was on addressing the onset phase in relation with the linear stability theory in forming quasi-singular current layers, in the plasmoid dominated regime for which the Lundquist number is higher than the critical value $S \gtrsim S_c$. Numerical simulations with FINMHD code are carried out at different magnetic Prandtl values in this high Lundquist number limit. The tilt mode is used as the initial setup to form the current layers on a fast ideal MHD time scale.

Our results confirm that, an onset phase characterized by a sudden super Alfvénic growth of plasmoids is obtained (with $\gamma_p \tau_A \simeq 10$ for our runs), as predicted by the stability theory proposed Comisso and collaborators ([Comisso & Grasso 2016](#); [Comisso et al. 2017](#)). The simple diagnostic using the time evolution of maximum current density is checked to be valid for this aim. During this phase, the plasmoids remain in a linear growth regime, and the transition to a non linear regime occurs when the statistical steady-state with oscillating current density is reached. This latter phase is characterized by a time-averaged reconnection rate nearly independent of the Lundquist number (see Paper I). Our results being very similar to the those obtained from the coalescence setup, suggest that Comisso et al.'s model is able to correctly predict the explosive growth of plasmoids leading to disruption of the reconnection current sheets when the initial configuration is ideally unstable. On the other hand, the other model developed by [Pucci & Velli \(2014\)](#), where the plasmoid linear growth is at most Alfvénic, could apply when the initial configuration is ideally

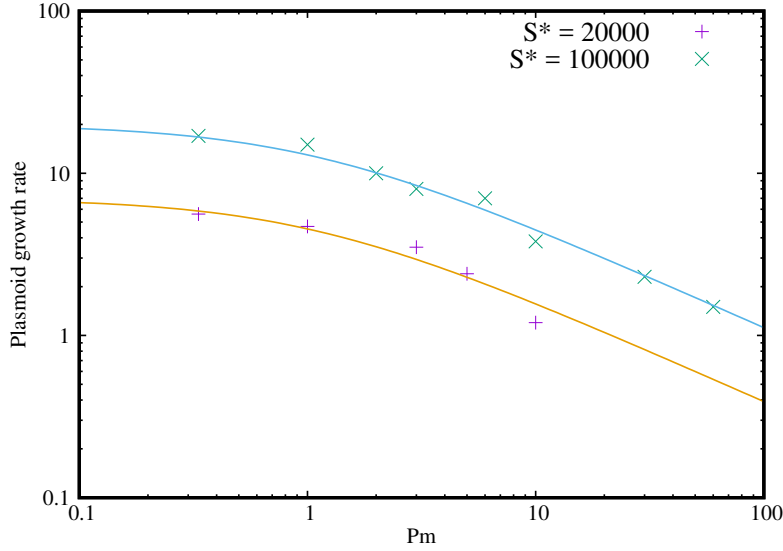


Figure 7. Plasmoid growth rate normalized to t_A^{-1} , i.e. $\gamma_p t_A$, obtained in different runs as a function of the magnetic Prandtl number P_m , for two inverse resistivity values ($S^* = 2 \times 10^4$ and 1×10^5). The theoretical dependences (see text) scaling as $(1 + P_m)^{-5/8}$ are plotted for comparison.

stable (and thus resistively unstable), as it has been validated using Harris-type current layer. This could explain the fastest time scale involved in the first category of setup (ideally unstable) compared to the second one (ideally stable).

The time-averaged normalized reconnection rate reported in Paper I is 0.014, that is two times higher than the value deduced from the coalescence setup. It is nevertheless in good agreement with values obtained in the literature of ~ 0.01 much higher than the Sweet-Parker rates, which could be sufficient to explain many disruptive events if the collisional regime apply. A fractal model (with hierarchical structure of the plasmoid chains that are effectively observed in simulations) based on heuristic arguments has been proposed to explain this fast rate independent of the Lundquist number (Huang & Bhattacharjee 2010). Indeed, to this end, a number of plasmoids (called non linear number) is required to scale linearly with S (Huang & Bhattacharjee 2010). Investigating this point is a complicated task requiring longer time simulations, and it will be the subject of a future study using tilt setup.

The Lundquist number reached in this study is high enough in order match the relevant values for tokamaks. Indeed, the relevant S value for the internal disruption associated with the internal kink mode is $S \simeq 10^5$, as $S = 0.004S^*$ ($S^* = 2.5 \times 10^7$ being a standard Lundquist number value defined in terms of the toroidal magnetic field) (Günter et al. 2015). The corresponding width of the Sweet-Parker current layer is thus estimated to be $a \simeq 1$ cm, and the smallest length scale associated to the plasmoid structure is probably of order 1 mm or even smaller, reaching thus a scale close to the kinetic ones. Kinetic effects could be incorporated to our model in order to address this point. For example, the plasmoid instability has been shown to facilitate the transition to a Hall reconnection in Hall magnetohydrodynamical framework with an even faster reconnection rate of ~ 0.1 (Huang et al. 2011). The smallest length scale associated to the plasmoid structure for $S = 10^6$ remains larger than the kinetic scale that is of order 10 m, when considering a solar loop structure and taking a length $L = 10^7$ m. However, as very high Lundquist number (at least 10^{10}) is required for the solar corona, kinetic effects could also play a role if the kinetic scale is reached via the plasmoid cascade at such huge Lundquist number.

REFERENCES

- BATY, H., & NISHIKAWA, H. 2016 Hyperbolic method for magnetic reconnection process in steady state magnetohydrodynamics. *MNRAS* **459** (1), 624–637, <https://doi.org/10.1093/mnras/stw654>
- BATY, H. 2019 FINMHD: An Adaptive Finite-element Code for Magnetic Reconnection and Formation of Plasmoid Chains in Magnetohydrodynamics. *The Astrophysical Journal Supplement Series* **243** (2), 23, <https://doi.org/10.3847/1538-4365/ab2cd2>
- BATY, H. 2020 Formation of plasmoid chains and fast magnetic reconnection during nonlinear evolution of the tilt instability. <https://ui.adsabs.harvard.edu/abs/2020arXiv200107036B/abstract>
- BHATTACHARJEE, A., HUANG, Y.-M., YANG, H., & ROGERS, B. 2009 Fast reconnection in high-Lundquist-number plasmas due to the plasmoid instability. *Phys. Plasmas* **16** (11), 112102, <https://doi.org/10.1063/1.3264103>
- COMISSO, L., & GRASSO, D. 2016 Visco-resistive plasmoid instability. *Phys. Plasmas* **23** (3), 032111, <https://doi.org/10.1063/1.4942940>

- COMISSO, L., LINGAM, M., HUANG, Y. M., & BHATTACHARJEE, A. 2016 General theory of the plasmoid instability. *Phys. Plasmas* **23** (10), 100702, <https://doi.org/10.1063/1.4964481>
- COMISSO, L., LINGAM, M., HUANG, Y. M., & BHATTACHARJEE, A. 2017 Plasmoid instability in forming current sheets. *The Astrophysical Journal* **850**, 142, <https://doi.org/10.3847/1538-4357/aa9789>
- GÜNTHER, S., YU, Q., LACKNER, K., BHATTACHARJEE, A., & HUANG, Y. M. 2015 Fast sawtooth reconnection at realistic Lundquist numbers. *Plasma Phys. Control. Fusion* **57** (1), 014017, <https://doi.org/10.1088/0741-3335/57/1/014017>
- HECHT, F. 2012 New development in FreeFem++. *Journal of Numerical Mathematics* **20**, 251-266, <https://doi.org/10.1515/jnum-2012-0013>
- HUANG, Y. M., COMISSO, L., & BHATTACHARJEE, A. 2017 Plasmoid instability in evolving current sheets and onset of fast reconnection. *The Astrophysical Journal* **849** (2), 75, <https://doi.org/10.3847/1538-4357/aa906d>
- HUANG, Y. M., & BHATTACHARJEE, A. 2010 Scaling laws of resistive magnetohydrodynamic reconnection in the high-Lundquist-number, plasmoid-unstable regime. *Phys. Plasmas* **17**, 062104, <https://doi.org/10.1063/1.3420208>
- HUANG, Y. M., BHATTACHARJEE, A., & SULLIVAN, B. P. A. 2011 Onset of fast reconnection in Hall magnetohydrodynamics mediated by the plasmoid instability. *Phys. Plasmas* **18**, 072109, <https://doi.org/10.1063/1.3606363>
- HUANG, Y. M., COMISSO, L., & BHATTACHARJEE, A. 2019 Scalings pertaining to current sheet disruption mediated by the plasmoid instability. *Phys. Plasmas* **26** (9), 092112, <https://doi.org/10.1063/1.5110332>
- KEPPENS, R., PORTH, O., GALSGAARD, K., ET AL. 2013 Resistive magnetohydrodynamic reconnection: Resolving long-term, chaotic dynamics. *Phys. Plasmas* **20** (9), 092109, <https://doi.org/10.1063/1.4820946>
- KEPPENS, R., PORTH, O., & XIA, C. 2014 Interacting tilt and kink instabilities in current channels. *The Astrophysical Journal* **795**, 77, <https://doi.org/10.1088/0004-637X/795/1/77>
- KNOLL, D. A., & CHACÓN, L. 2006 Coalescence of magnetic islands, sloshing, and the pressure problem. *Phys. Plasmas* **13** (3), 032307, <https://doi.org/10.1063/1.2173515>
- LANKALAPALLI, S., FLAHERTY, J. E., SHEPHARD, M. S., & STRAUSS, H. R. 2007 An adaptive finite element method for magnetohydrodynamics. *Journal of Computational Physics* **225** (1), 363-381, <https://doi.org/10.1006/jcph.1998.6091>
- LOUREIRO, N. F., SCHEKOCIHIN, A. A., & COWLEY, S. C. 2007 Instability of current sheets and formation of plasmoid chains. *Phys. Plasmas* **14** (10), 100703, <https://doi.org/10.1063/1.2783986>
- LOUREIRO, N. F., SAMTANEY, R., & UZDENSKY, D. A. 2012 Magnetic reconnection and stochastic plasmoid chains in high-Lundquist-number plasmas. *Phys. Plasmas* **19** (4), 042303, <https://doi.org/10.1063/1.3703318>
- NG, C. W., ROSENBERG, D., GERMASCHEWSKI, K., POUQUET, A., & BHATTACHARJEE, A. 2007 A comparison of spectral element and finite difference methods using statically refined nonconforming grids for the MHD island coalescence instability problem. *The Astrophysical Journal Supplement Series* **177** (2), 613-625, <https://doi.org/10.1086/588139>
- SAMTANEY, R., LOUREIRO, N. F., UZDENSKY, D. A., SCHEKOCIHIN, A. A., & COWLEY, S. C. 2009 Formation of plasmoid chains in magnetic reconnection. *Phys. Rev. Lett.* **103** (10), 105004, <https://doi.org/10.1103/PhysRevLett.103.105004>
- SWEET, P. A. 1958 The neutral point theory of solar flares. In *Electromagnetic Phenomena in Cosmical Physics* (ed. Lehnert B). p. 123. Cambridge: Cambridge University Press.
- PARK, MONTICELLO, D. A., AND WHITE, R. B. 1984 Reconnection rates of magnetic fields including the effects of viscosity. *Phys. Fluids* **27**, 137, <https://doi.org/10.1063/1.864502>
- PARKER, E. N. 1957 Sweet's mechanism for merging magnetic fields in conducting fluids. *J. Geoph. Research.* **62**, 50520, <https://doi.org/10.1029/JZ062i004p00509>
- PHILIP, B., PERNICE, M., & CHACON, L. 2007 Solution of reduced resistive magnetohydrodynamics using implicit adaptive mesh refinement. *Lecture Notes in Computational Science and Engineering* **55**, 723-729, https://doi.org/10.1007/978-3-540-34469-8_90
- PRIEST, E. R., & FORBES, T. G. 2000 Magnetic Reconnection. (Cambridge: Cambridge Univ. Press), <https://doi.org/10.1017/CBO9780511525087>
- PUCCI, F., & VELLI, M. 2014 Reconnection of quasi-singular current sheets: the 'ideal' tearing mode. *The Astrophysical Journal Letters* **780** (2), L19, <https://doi.org/10.1088/2041-8205/780/2/L19>
- PUCCI, F., VELLI, M., TENERANI, A., & DEL SARTO, D. 2018 Onset of fast ideal tearing in thin current sheets: Dependence on the equilibrium current profile. *Phys. Plasmas* **25** (3), 032113, <https://doi.org/10.1063/1.5022988>
- RICHARD, R. L., SYDORA, R. D., & ASHOUR-ABDALLA, M. 1990 Magnetic reconnection driven by current repulsion. *Phys. Fluids B* **2**, 488-494, <https://doi.org/10.1063/1.859338>
- RIPPERDA, B., PORTH, O., XIA, C., & KEPPENS, R. 2017 Reconnection and particle acceleration in interacting flux ropes I. Magnetohydrodynamics and test particles in 2.5D. *MNRAS* **467**, 3279-3298, <https://doi.org/10.1093/mnras/stx379>
- STRAUSS, H. R., & LONGCOPE, D. W. 1998 An Adaptive Finite Element Method for Magnetohydrodynamics. *Journal of Computational Physics* **147** 318, <https://doi.org/10.1006/jcph.1998.6091>
- TENERANI, A., VELLI, M., RAPAZZO, A. F., & PUCCI, F. 2015 Magnetic reconnection: recursive current sheet collapse triggered by 'ideal' tearing. *The Astrophysical Journal Letters* **813**, L32, <https://doi.org/10.1088/2041-8205/813/2/L32>
- TENERANI, A., VELLI, M., PUCCI, F., LANDI, S., M., AND RAPAZZO, A. F. 2016 'Ideally' unstable current sheets and the triggering of fast magnetic reconnection. *Journal of Plasma Physics* **82** (5), 535820501, <https://doi.org/10.1017/S002237781600088X>
- TOLMAN, E. A., LOUREIRO, N. F., & UZDENSKY, D. A. 2018 Development of Tearing Instability in a Current Sheet Forming by Sheared Incompressible Flow. <https://doi.org/10.1017/S002237781800017X>
- UZDENSKY, D. A., LOUREIRO, N. F., & SCHEKOCIHIN, A. A. 2010 Fast magnetic reconnection in the plasmoid-dominated regime. *Phys. Rev. Lett.* **105** (23), 235002, <https://doi.org/10.1103/PhysRevLett.105.235002>
- UZDENSKY, D. A., LOUREIRO, N. F., SCHEKOCIHIN, A. A. 2010 Magnetic reconnection onset via disruption of a forming current sheet by the tearing instability. *Phys. Rev. Lett.* **116** (10), 105003, <https://doi.org/10.1103/PhysRevLett.116.105003>